JACS
JOURNAL OF THE AMERICAN CHEMICAL SOCIETY

ARTICLE

pubs.acs.org/JACS

Silicon Nanowire Fabric as a Lithium Ion Battery Electrode Material

Aaron M. Chockla,[†] Justin T. Harris,[†] Vahid A. Akhavan,[†] Timothy D. Bogart,[†] Vincent C. Holmberg,[†] Chet Steinhagen,[†] C. Buddie Mullins,[†,‡] Keith J. Stevenson,[‡] and Brian A. Korgel[†,*]

[†]Department of Chemical Engineering and [‡]Department of Chemistry and Biochemistry, Texas Materials Institute, Center for Nano- and Molecular Science and Technology, The University of Texas at Austin, Austin, Texas 78712-1062, United States

Supporting Information

ABSTRACT: A nonwoven fabric with paperlike qualities composed of silicon nanowires is reported. The nanowires, made by the supercritical-fluid−liquid−solid process, are crystalline, range in diameter from 10 to 50 nm with an average length of >100 μm, and are coated with a thin chemisorbed polyphenylsilane shell. About 90% of the nanowire fabric volume is void space. Thermal annealing of the nanowire fabric in a reducing environment converts the polyphenylsilane coating to a carbonaceous layer that significantly increases the electrical conductivity of the material. This makes the nanowire fabric useful as a self-supporting, mechanically flexible, high-energy-storage anode material in a lithium ion battery. Anode capacities of more than 800 mA h g^{-1} were achieved without the addition of conductive carbon or binder.

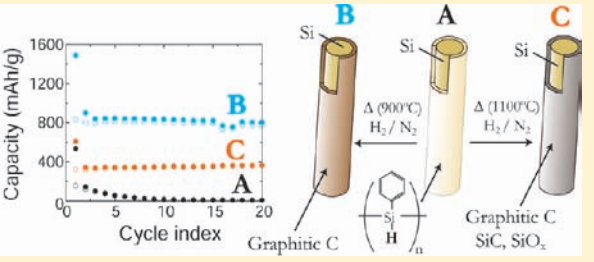

INTRODUCTION

The demand for portable electronic devices has been steadily rising, in part because of the increasing global dependence on mobile information, entertainment, and communication. These devices require portable power sources. Lithium ion (Li^+) batteries (LIBs) have become widely used because of their high energy density, but there is a strong desire to improve many aspects of LIBs, including cost, safety, energy density, capacity, cycle life, and rate capability.[1] The recent interest in using LIBs in automobiles has heightened the search for new materials that can achieve higher energy density and prolonged cycle life.[2]

A LIB functions by shuttling Li^+ between the anode and cathode. The typical cathode in a commercially available LIB is composed of lithium metal oxide (i.e., $LiCoO_2$) and the anode of graphite. The LIB capacity is limited in part by the intercalation of Li^+ by the graphitic anode material; thus, higher capacity batteries require anode materials that can accommodate more Li^+. The theoretical capacity of the graphite anode is 372 mA h g^{-1}.[3,4] Lithium-alloying materials have the potential for significantly higher storage capacities. For instance, Si alloys with Li^+ at room temperature to form $Li_{15}Si_4$, which corresponds to a substantially higher theoretical capacity of 3579 mA h g^{-1}.[5−7] However, Si undergoes an enormous volume expansion of nearly 300% when fully lithiated.[8] Bulk crystalline Si cannot tolerate the stresses associated with these lithation/delithiation cycles and crumbles, resulting in battery failure.[9] On the other hand, Si nanostructures have been found to tolerate extreme changes in volume with cycling.[7,10−21] Thin Si films have realized capacities above 2000 mA h g^{-1}.[12,13,19] Si nanoparticles have also been explored, but with overall specific capacities that have been limited by the need for a conductive carbon matrix to ensure electrical contact with the electrode.[11,18] Si nanowires have been promising.[7,14−17,20,21] For example, Cui and co-workers achieved a capacity of 2725 mA h g^{-1} with very good stability, retaining more than 1400 mA h g^{-1} after 700 cycles using an interconnected amorphous Si hollow nanosphere thin-film electrode.[22] Unfortunately, these electrode materials are very expensive at present and cannot be produced in the significant quantities needed for commercial LIB applications.[12,13,19]

Solvent-based processes for nanowire synthesis, such as supercritical-fluid−liquid−solid (SFLS) and solution−liquid−solid (SLS) growth, can produce large amounts of Si nanowires (SiNWs) at relatively low cost.[23−28] In a 10 mL laboratory-scale reactor, hundreds of milligrams of nanowires with lengths of >100 μm can be produced in a few hours,[23,26] which is sufficient to create nanowire-based nonwoven fabrics several inches on a side.[27] These nanowires exhibit excellent mechanical properties, are highly flexible, and have strength-to-weight ratios greater than those of both carbon fiber and Kevlar.[27,29] This fabric material is thin (thickness of 50−150 μm) and has a paperlike appearance and feel. The first fabrics consisting entirely of one-dimensional nanomaterials were made from carbon nanotubes (CNTs) because of their mechanical strength, flexibility, and large aspect ratio and the ability to produce the material in macroscopic quantities.[30,31] Metal oxide nanowires of cryptomelane-M ($K_{2-x}Mn_8O_{16}$) that could be synthesized in large quantities by hydrothermal methods have been used to form macroscopic free-standing membranes.[32] Recently, SFLS synthesis has been used to produce Ge nanowire fabric.[27,33] Fabric-like materials consisting of CNTs and graphene sheets have recently been explored as electrodes for flexible

Received: September 2, 2011
Published: November 09, 2011

LIB applications[11,21,34−37] and as electrode supports for other materials, as in graphene−silicon,[11,37] CNT−SiNW,[21,34] and CNT−$Li_4Ti_6O_{12}$[21,35] electrodes. Here we demonstrate the creation of a Si nanowire fabric and show that it can function as a standalone anode material without the need for additional conductive fillers (activated carbon) or polymeric binders. For good battery performance, it was necessary to convert a thin polyphenylsilane[38] coating on the Si nanowires to carbon by annealing under forming gas (7% H_2 in N_2) at 900 °C. This thin layer provides the electrical conductivity needed for efficient Li^+ charging and discharging of the layer. The LIB performance of the Si nanowire fabric and the role of the shell on the cycling behavior are reported.

EXPERIMENTAL SECTION

Materials. All chemicals were used as received without further purification. Dodecanethiol (DDT, ≥98%), hydrogen tetrachloroaurate trihydrate (≥99.9%), sodium borohydride (≥98%), toluene (anhydrous, ACS grade, 99.8%), ethanol (99.9%), tetraoctylammonium bromide (TOAB, 98%), and chloroform (99.8%) were purchased from Sigma-Aldrich. Monophenylsilane (MPS, >95%) was obtained from Gelest, and $LiPF_6$ [1.0 M in a 1:1 ethylcarbonate (EC, >99.95%)/ diethyl carbonate (DEC, >99.98%) mixture] was purchased from Novolyte. For battery assembly, Celgard 2400 membranes (25 μm, purchased from Celgard) were used as separators, and Li metal (99.9%) was obtained from Alfa Aesar.

Silicon Nanowire Synthesis. Si nanowires were synthesized by gold nanocrystal-seeded SFLS growth in toluene using the synthetic procedures detailed in previous reports.[38] Briefly, MPS and 2 nm Au nanoparticles[39] were mixed together in a 290:1 Si:Au mole ratio and diluted with anhydrous toluene to achieve an MPS concentration of 156 mM. Nanowires were then grown in a flow-through sealed titanium reactor at 490 °C and 10.3 MPa. After the reaction, the nanowires were collected from the reactor walls and washed with chloroform (10 mL) and ethanol (5 mL) several times via centrifugation at 8000 rpm. The nanowires were then dispersed in chloroform to a concentration of 5 mg/mL and stored in a vial under ambient conditions prior to use.

Material Characterization. Scanning electron microscopy (SEM) images were acquired using a Zeiss Supra 40 scanning electron microscope with an in-lens arrangement, a working voltage of 5 keV, and a working distance of 5 mm. SEM samples were imaged on silicon wafers obtained from SEH. Transmission electron microscopy (TEM) images were digitally acquired using either a FEI Tecnai Spirit BioTwin transmission electron microscope operated at 80 kV or a JEOL 2010F field-emission microscope operated at 200 kV. TEM samples were prepared by drop-casting from chloroform dispersions onto 200 mesh lacey carbon copper TEM grids (Electron Microscopy Sciences).

X-ray diffraction (XRD) was carried out using a Rigaku R-Axis Spider diffractometer with an image-plate detector and Cu Kα radiation (λ = 1.5418 Å) operated at 40 kV and 40 mA. Measurements were taken on samples on a 0.5 mm nylon loop. Samples were scanned for 10 min while rotating at 1 deg/s under ambient conditions. The radial data were integrated from 2θ = 20 to 80° and plotted. Background scattering from the nylon loop was subtracted from the sample measurement.

X-ray photoelectron spectroscopy (XPS) was performed on a Kratos photoelectron spectrophotometer with monochromatic Al Kα radiation (1487 eV). The Si nanowire fabric was secured on the experimental tray using double-sided Cu tape. Spectra were collected at 0.1 eV intervals using an integration time of 800 ms through a tungsten coil set at 4.8 V bias with respect to the sample. Data were collected continuously under high vacuum (10^{-9} Torr). The effect of sample charging on the XPS data was corrected by shifting the Si^0 $2p_{3/2}$ peak to a binding energy of 99.3 eV.

The XPS results were analyzed using CasaXPS software. Background subtraction was done using a Shirley background model. Peak areas were deconvoluted as Voigt functions (30% Gaussian character). The Si 2p region was deconvoluted as Si^0 $2p_{3/2}$, Si^0 $2p_{1/2}$, Si^+, Si^{2+}, Si^{3+}, and Si^{4+} peaks placed at 99.3, 99.9, 100.1, 101.1, 102.1, and 103.2 eV, respectively. The zero-valent Si spin splits were assumed to have the same full width at half-maximum (FWHM), and the area of the $2p_{1/2}$ peak was set as half the area of the $2p_{3/2}$ peak. Similarly, one FWHM value was used for all of the other oxide peaks; however, for simplicity, the other oxidative states were not divided into their respective spin splits. Values for the FWHM of the oxidized states were constrained by placing the FWHM between 1.8 and 2.2 times the zero-valent peaks.

The C1s region was deconvoluted into three peaks placed at 284, 284.7, and 285.5 eV. These binding energies correspond to Si−C, C−C, and C−O bonding, respectively. The O 1s region was deconvoluted into two peaks. The first peak, placed at 532.5 eV, corresponds to SiO_2 and C−O bonding. The second peak, placed at 533.9 eV, relates to O_2 adsorbed on the surface of the wires. Only one FWHM was used to generate the peaks for each species of C and O.

Raman spectroscopy was performed using a Renishaw inVia microscope equipped with a 514.5 nm argon ion laser in backscattering configuration. The Stokes Raman signal at 521 cm^{-1} for single-crystalline bulk Si oriented with the [110] direction normal to the laser was used to calibrate the instrument. The beam was focused using an optical microscope with a 50× objective lens. Spectra were taken on free-standing sheets of nanowire fabric lying on glass slides by single scans from 100 to 2000 cm^{-1} at 5% laser power (0.2 mW).

LIB Anode Processing and Battery Testing. Si nanowire fabric was prepared by sonicating nanowire dispersions (5−10 mg/mL Si nanowires in chloroform) for 1 h. The dispersions were drop-cast into a Teflon trough and left overnight to dry. After drying, the fabric was peeled from the trough using tweezers (and a thin razor blade wedged between the fabric and trough bed when necessary; see movie S1 in the Supporting Information) and cut into 1 cm × 1 cm squares that were loaded into quartz boats and heated under a moderate flow of forming gas in a tube furnace.

Batteries were prepared within an argon-filled glovebox using a Cu foil current collector. The Si nanowire fabric was placed on the Cu current collector to serve as the anode material. The electrolyte was a 1.0 M solution of $LiPF_6$ in a 1:1 EC (>99.95%):DEC (>99.98%) mixture (Novolyte). A few drops of electrolyte were deposited over the nanowire fabric. A Celgard 2400 separator membrane (25 μm thick) was then added, followed by Li metal foil (99.9%, Alfa Aesar) as the counter electrode. Galvanostatic measurements were made using an Arbin BT-2143 test unit that was cycled between 3 V and 10 mV vs Li/Li^+ at a rate of C/20 (C = 3579 mA h g^{-1} [5−7]).

After cycling, the batteries were disassembled, and the anode was cleaned by soaking the fabric in acetonitrile overnight and then rinsing with 0.5 M sulfuric acid for 1 min (i.e., until bubbling subsided). The anode was then placed in a vial and soaked in isopropyl alcohol (IPA) for several minutes. The IPA was decanted, and the anode was soaked two more times in the same way and then dried in air before SEM and TEM imaging.

RESULTS AND DISCUSSION

Si Nanowire Fabric. Figure 1 shows a photograph and SEM images of Si nanowire fabric made by casting concentrated dispersions of SFLS-grown nanowires in toluene into a Teflon trough (See movie S1 in the Supporting Information). The fabric is composed of highly entangled nanowires. It is ∼50 μm thick and relatively porous, containing ∼90% void volume. The Si nanowire fabric is pliable with good mechanical integrity (see movie S2 in the Supporting Information). Even though the

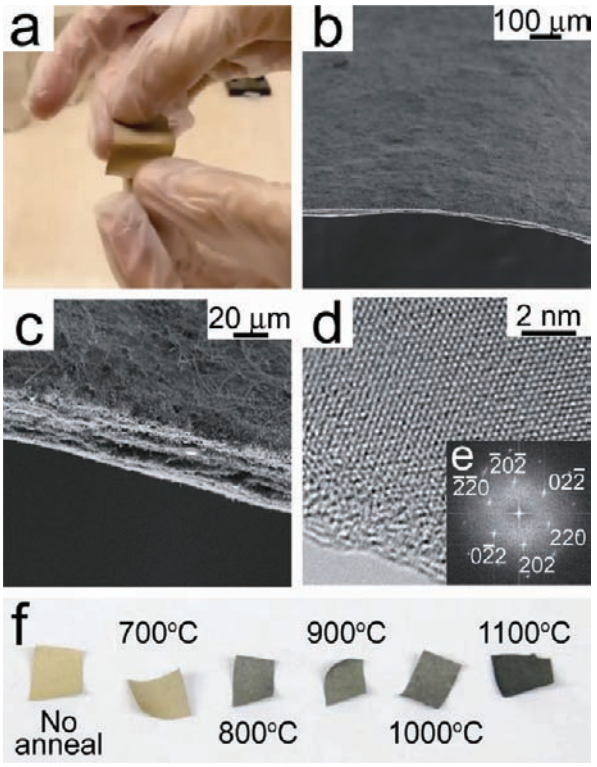

Figure 1. (a) Photograph of mechanically flexible Si nanowire fabric. (b, c) SEM images of the fabric. (d) High-resolution TEM (HRTEM) image of a Si nanowire showing its crystallinity. (e) Fast Fourier transform (FFT) pattern from the HRTEM image in (d) showing a ⟨110⟩ growth direction. (f) Photographs of Si nanowire fabrics annealed at the indicated temperatures under a reducing atmosphere.

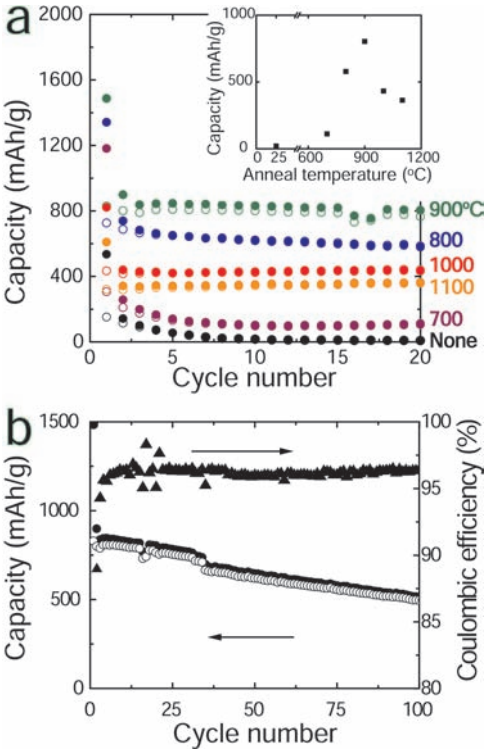

Figure 2. (a) Galvanostatic cycling tests of Si nanowire fabric before and after annealing at 700, 800, 900, 1000, and 1100 °C at a cycle rate of $C/20$ (C = 3579 mA h g^{-1} [5–7]). The inset shows discharge capacities after 20 cycles for batteries with nanowire fabric anodes annealed at various temperatures. (b) Galvanostatic cycling of a Si nanowire fabric anode annealed at 900 °C.

nanowires are single crystals of a material (i.e., Si) that is brittle in bulk form, they are mechanically flexible and strong because of their narrow diameter.[27]

Electrochemical Performance of Si Nanowire Fabric Anodes in LIBs. 1 cm × 1 cm squares of Si nanowire fabric were tested as standalone Si-based anode materials without added conductive carbon or binder for a LIB. The as-made Si nanowire fabric performed poorly. As shown in Figure 2a, the capacity in the first cycle was just under 600 mA h g^{-1} but then dropped to nearly zero after only a couple of cycles. Tests of the electrical conductivity showed that the nanowire fabric is electrically insulating with a conductivity of ∼0.2 nS/m. The nanowire fabric must be sufficiently conductive to facilitate efficient lithium alloying with Si.[40]

The electrical conductivity of the Si nanowire fabric was enhanced significantly by annealing under a reducing atmosphere at temperatures greater than 700 °C. Figure 3 shows current−potential curves for nanowire fabric annealed at various temperatures. Annealing at temperatures between 700 and 1000 °C led to conductivities ranging from 70 to 150 nS/m. Fabric annealed at 1100 °C had a conductivity of 1400 nS/m.

Figure 1f shows photographs of Si nanowire fabric after annealing under forming gas at various temperatures. The fabric turns increasingly black with increasing annealing temperature. The Si nanowires produced by the SFLS process using phenylsilane as a reactant have a thin polyphenylsilane shell on their surface.[38] Annealing under a reducing environment transforms this shell material to carbon, which provides the significantly

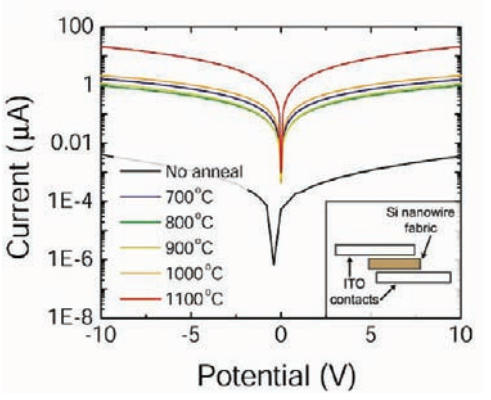

Figure 3. Current−potential measurements of Si nanowire fabric placed between two indium tin oxide (ITO) electrodes (inset). The nanowire fabric was annealed under a reducing atmosphere at the indicated temperatures. Measurements were made using ∼150 μm thick fabric samples with a contact area of 1 cm^2.

enhanced electrical conductivity. When the nanowires are annealed in the presence of oxygen and water, the shell material oxidizes to a defective and insulating SiO_2 layer.

The annealed Si nanowire fabric performed well in galvanostatic cycling tests. Figure 2a shows the capacity (with cycling at a $C/20$ rate, where C = 3579 mA h g^{-1}, corresponding to $Li_{15}Si_4$ [5–7]) for Si nanowire fabric annealed under a reducing atmosphere at

Table 1. Summary of the Capacity Retention Data for Si Nanowire Fabric Anodes Annealed at the Indicated Temperatures

	capacity (mA h g^{-1})			retention (%)	
temperature (°C)	1st cycle	2nd cycle	20th cycle	C_{ret1} [a]	C_{ret2} [b]
no anneal	534	142	8	2	6
700	1180	257	111	9	43
800	1341	738	579	43	78
900	1485	898	804	54.0	89
1000	821	439	433	57	99
1100	608	341	363	60	106

[a] Amount of charge capacity retained after 20 cycles relative to the first charging cycle. [b] Amount of charge capacity retained after 20 cycles relative to the second charging cycle.

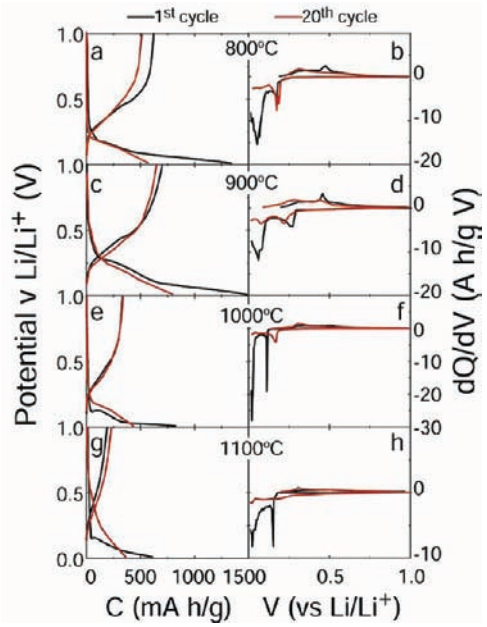

Figure 4. Constant-current voltage profiles for Si nanowire fabric anodes annealed at (a) 800, (c) 900, (e) 1000, and (g) 1100 °C with corresponding differential capacity curves (b, d, f, and h, respectively).

various temperatures. All of the nanowire samples exhibited a large initial irreversible capacity loss during the first cycle, which is typical for Si anode materials and results from formation of solid−electrolyte interface (SEI) layers upon cycling to low potentials. The nanowire fabric annealed to 700 °C performed better than the as-made nanowires, but the capacity was still very limited. On the other hand, nanowires annealed at 900 °C performed quite well and retained a cycling capacity of 800 mA h g^{-1} after 20 cycles. As shown in Figure 2b, the capacity was still higher than 500 mA h g^{-1} after 100 cycles. When the nanowires were annealed at even higher temperature (>900 °C), they did not perform as well. The Figure 2a inset shows a plot of the discharge capacity after 20 cycles for Si nanowire fabric electrodes annealed at various temperatures. The highest performance was achieved with nanowires annealed at 900 °C. Table 1 summarizes the capacity retention data of the Si nanowire fabric annealed at various temperatures.

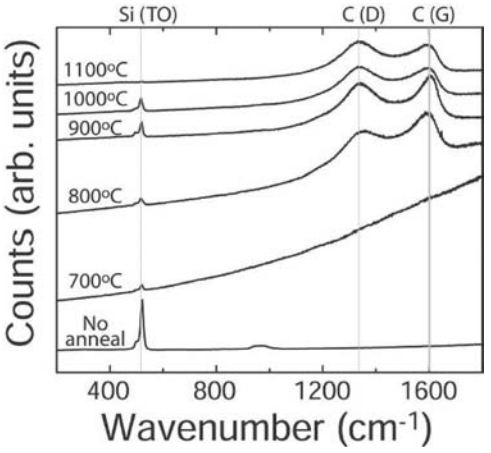

Figure 5. Raman spectra of Si nanowire fabric before and after annealing under a reducing atmosphere at various temperatures. The Si (TO) peak at 521 cm^{-1} and carbon-related D and G bands at 1380 and 1560 cm^{-1} are labeled.

Figure 4 shows the constant-current voltage profiles and differential capacity (dQ/dV) curves for the first and 20th cycles of batteries with Si nanowires annealed at 800, 900, 1000, and 1100 °C. Each constant-current voltage profile shows two plateaus during the charge cycle, corresponding to the lithiation of crystalline silicon and the formation of the $Li_{15}Si_4$ phase.[6] The discharge cycles have a steeper slope than the charge cycles (corresponding to a broader peak in the dQ/dV curves), indicating that delithiation occurs over a relatively broad range of potentials, which is consistent with amorphous silicon. The dQ/dV plots provide a better illustration of the potentials at which the lithiation and delithiation events occur. Each of the first-cycle charge curves in the dQ/dV plots shows a peak between 150 and 200 mV, corresponding to lithiation of crystalline Si. This peak is shifted slightly in the 900 °C sample (Figure 4d) to ∼250 mV. A peak near 50 mV is also observed for each sample and is attributed to the formation of $Li_{15}Si_4$.[6] By the 20th cycle, the first lithiation event has shifted to ∼300 mV, which falls in the range expected for lithiation of amorphous Si (a-Si).[41] The second lithiation event has a significantly reduced intensity, indicating a marked consumption of crystalline silicon. The first discharge cycle shows a prominent peak at ∼450 mV, which corresponds to the delithiation potentials of amorphous silicon and $Li_{15}Si_4$.[41] Lithium extraction during the 20th cycle occurs at the a-Si delithiation potential (300 mV).[41]

Composition of the Carbonaceous Shell on the Si Nanowires. Raman spectroscopy, XPS, and XRD were used to determine the composition of the shell material formed after annealing the nanowires under forming gas. Figure 5 shows Raman spectra of nanowires as-made and after annealing at various temperatures. The as-made nanowires exhibit the characteristic Si (TO) band at 521 cm^{-1} along with a smaller peak at 495 cm^{-1} that is most likely related to stacking faults.[42−45] After annealing of the nanowires at 700 °C, the nanowire spectra still have the characteristic Si-related peaks, but there is a significant sloping baseline due to fluorescence from the sample. This fluorescence is due to a chemical change in the shell material that is probably related to the phenyl species. With increasing annealing temperature, the fluorescence signal diminishes in intensity. Nanowires annealed at 900 °C and above have almost no fluorescent background. The nanowires annealed at 800 °C

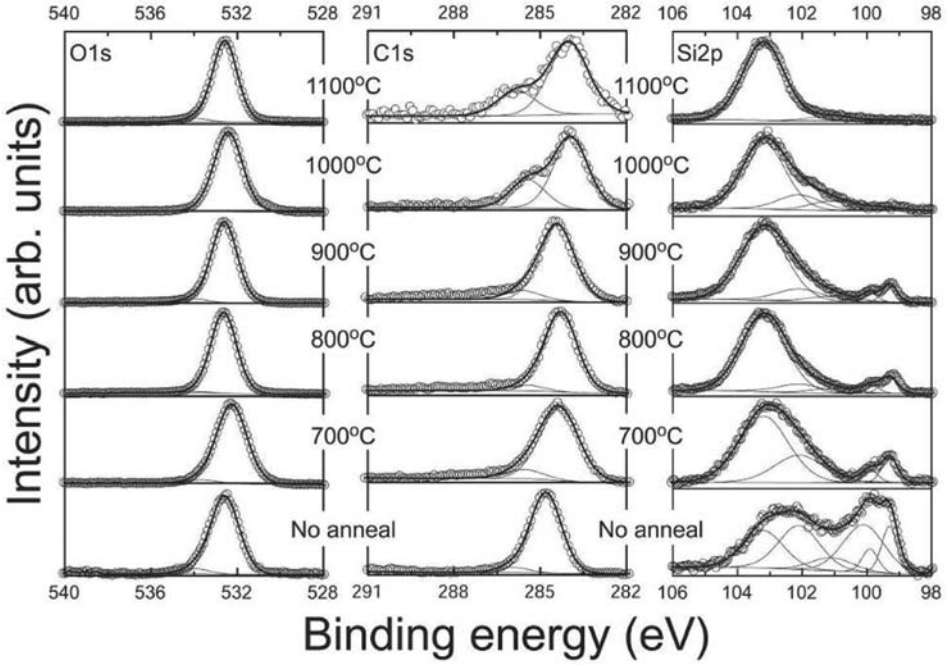

Figure 6. XPS data for the O 1s, C 1s, and Si 2p states of Si nanowire fabric annealed at the indicated temperatures. The intensities of all of the peaks are normalized, but the carbon signal decreases significantly relative to the Si signal as the annealing temperature increases. Figure 7 plots the relative amounts of O, C, and Si obtained from integration of the XPS peaks. The peak-fitting procedures are described in the Experimental Section.

and higher exhibit two prominent bands at ~1350 and ~1600 cm^{-1}, corresponding to disordered (D) and graphitic (G) carbon.[46−49] These peaks are not present in the Raman spectra of the as-made nanowires nor in the spectra of the nanowires annealed at 700 °C. It appears that the fluorescent species formed as a result of annealing at 700 °C is converted to the carbon that forms at higher annealing temperatures.

The much improved battery performance of the Si nanowire fabric after annealing results from the formation of the electrically conductive carbon layer on the nanowires. It is obvious from the change in color of the nanowire fabric from its typical pale-yellow to black that the shell material has been converted to carbon, as confirmed by the Raman spectra. But why does the battery performance diminish when the nanowires are heated above 900 °C? The Raman spectra show that the same carbon species that helped to achieve good battery response are still present on the nanowires annealed at 1000 and 1100 °C, and the electrical conductivity of the nanowires is also high (Figure 3). However, XPS (Figures 6 and 7) and XRD (Figure 8) reveal that a significant amount of Si oxidation and some SiC formation occur when the nanowires are annealed at these higher temperatures. The XRD patterns in Figure 8 show that the nanowires are still composed predominantly of crystalline Si after annealing, indicating that the oxidation and carbide formation occurs only on the nanowire surface. It appears that residual oxygen or water, most likely contained initially in the polyphenylsilane shell, oxidizes the surfaces of the nanowires. Nanowires annealed at 1100 °C no longer have a measurable Si^0 XPS peak, and all of the Si signal corresponds to either Si^{4+} or Si^{2+}. XRD also indicates that some of the surface carbon reacts with the underlying Si to form SiC. The SiC diffraction peaks are very broad, indicating that the crystalline SiC domains are extremely small, which is consistent with the lack of a SiC-related Raman signal at 790 cm^{-1}.[50] The Si^0 signal does not show up in the XPS or Raman spectra because the surface layer becomes too thick to penetrate. Additionally, there is a noticeable decrease in the relative carbon signal in the XPS spectra, along with the appearance of a relatively strong XPS signal at higher binding energy of 285.5 eV, indicating that the carbonaceous layer has also oxidized to some extent (Figures 6 and 7).

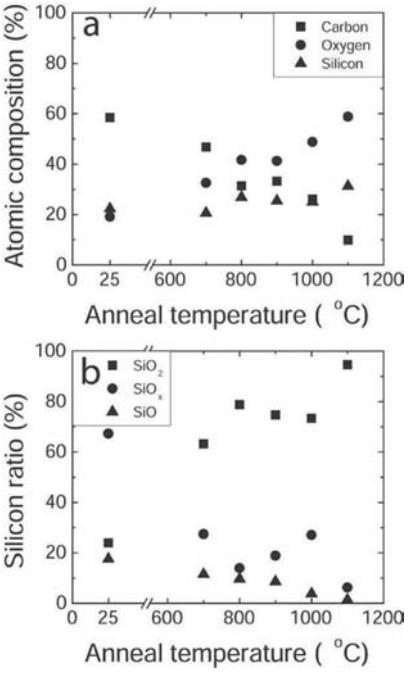

Figure 7. Summary of compositional analyses extracted from the XPS data in Figure 6: (a) relative Si, C, and O content determined by integrating the O 1s, C 1s, and Si 2p peaks; (b) relative SiO, SiO_x, and SiO_2 content determined from the Si 2p peak structure.

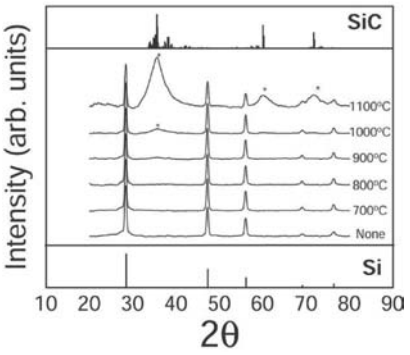

Figure 8. XRD patterns of Si nanowire fabric before and after annealing at the indicated temperatures under forming gas. The peak positions corresponding to diamond cubic Si (JCPDS no. 00-027-1402) and silicon carbide (SiC, labeled with *; JCPDS no. 00-029-1131) are shown.

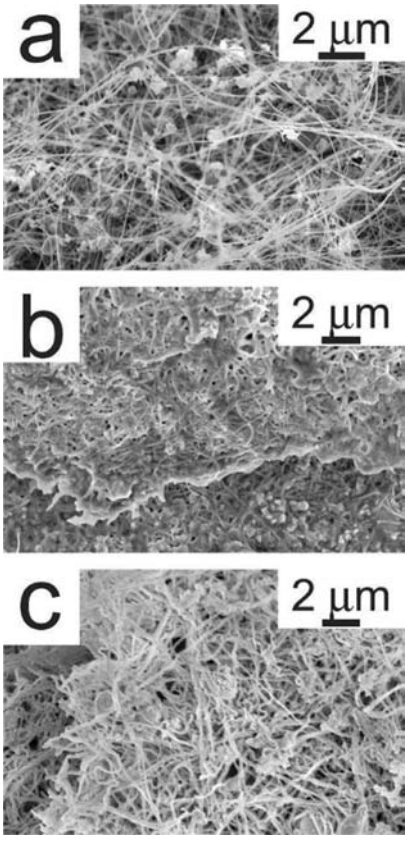

Figure 9. SEM images of Si nanowire fabric annealed at 900 °C under forming gas (a) prior to electrochemical cycling, (b) after 20 galvanostatic cycles without washing, and (c) after 20 galvanostatic cycles with washing using acetonitrile, H_2SO_4, and IPA.

The oxide and SiC that forms at the nanowire surface after annealing at 1000 and 1100 °C is most likely responsible for the reduced lithiation/delithiation of the nanowire fabric. SiC is known to be electrochemically inactive for lithiathion,[51] and the oxide layer creates an electrically insulating barrier between the Si core and the electrolyte that is not conducive to battery performance.

Si Nanowire Structure after Electrochemical Cycling. The coin cell housing was disassembled after cycling to examine the structural integrity of the nanowires by SEM and TEM. Figure 9 shows SEM images of the Si nanowire fabric that had been annealed at 900 °C under forming gas before and after 20 galvanostatic cycles. The nanowires removed from the coin cell housing were covered with an organic surface coating, presumably comprised of $ROCO_2Li$ and ROLi species associated with reduction of the EC/DEC solvent.[14] Rinsing the nanowires with acetonitrile, H_2SO_4, and IPA removed the organic coating (SEI layer). In comparison with the nanowires prior to electrochemical cycling, the nanowires appear to be larger in diameter. TEM images of the nanowires after galvanostatic cycling showed two different populations of nanowires in nearly equal proportions. As shown in Figure 10, some nanowires were amorphous and appeared to have hollowed cores. Others had a crystalline core with a thick amorphous shell. Nanoprobe energy-dispersive spectroscopy (EDS) maps of Si, O, and C composition across the nanowire diameters showed that nanowires with crystalline cores had a higher concentration of Si in the center, with a measurable amount of carbon and oxygen mostly at the nanowire surface. The amorphous nanowires with the hollow cores had a high concentration of Si in the shell, along with C and O. It appears that the structural integrity of these Si nanowires was lost during lithium cycling, with a rupture of the shell. The presence of the nanowires with crystalline cores may indicate that these

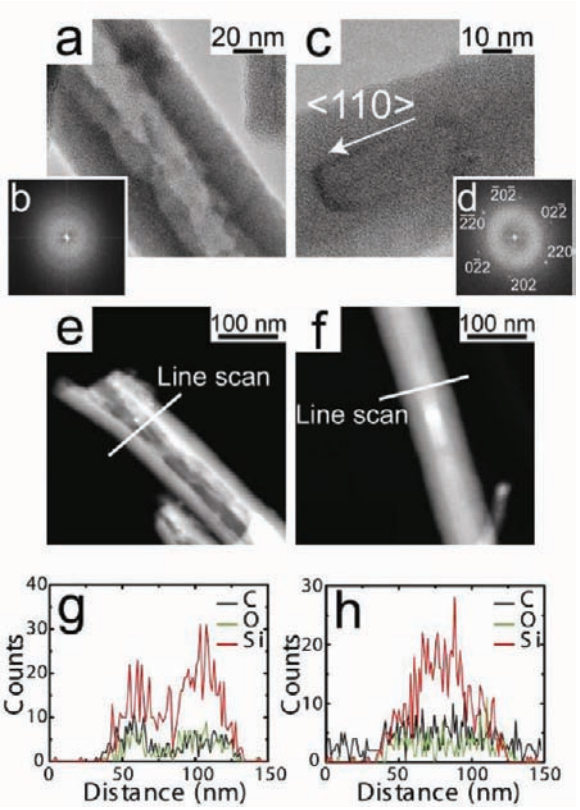

Figure 10. TEM and scanning TEM (STEM) images of Si nanowires annealed at 900 °C under forming gas after 20 electrochemical cycles in a lithium cell. (a, c) Two types of nanowires were observed in nearly equal proportions: (a) amorphous wires that appear to have a hollow core and (c) crystalline nanowires with a thick amorphous shell. (b, d) FFTs of the TEM images in (a) and (c). (e, f) STEM images and (g, h) corresponding EDS line scans at the indicated positions of (e, g) amorphous wires that appear to have a hollow core and (f, h) crystalline nanowires with a thick amorphous shell.

nanowires were not involved in the electrochemical cycling. These issues require further study.

CONCLUSION

A nonwoven fabric of Si nanowires has been reported. The fabric has the look and feel of tissue paper yet is composed entirely of crystalline Si. Annealing the nanowire fabric at 900 °C under reducing atmosphere (forming gas) leads to good performance as an anode in a Li^+ battery without addition of carbon binder. The key to their good performance is the presence of a thin electrically conductive carbon layer on the nanowires. When the nanowires were annealed above 900 °C, the battery performance diminishes because of the formation of a surface barrier layer of SiO_2 and SiC under the conducting carbonaceous coating that prevents efficient lithitation and delithiation.

This study has shown that the surface composition of Si nanowires plays a critical role in their effectiveness as an anode material in an LIB. Si nanowires can alloy with lithium, but their capacity and cycling stability all rely on the quality of the surfaces. In the present case of Si nanowires grown by the SFLS process with monophenylsilane as a reactant, a residual polyphenylsilane shell can be converted from an inactive layer to a coating that enables Si nanowire lithiation/delithiation. The coating is conformal and uniform and does not require a separate materials deposition step. Carbon binder, which would lower the specific capacity of the material, need not be added. This Si nanowire fabric represents a mechanically flexible silicon anode material with the potential to be applied in lightweight paper-based or plastic LIBs. Future research needs to focus on understanding the cycling durability and the factors that limit performance, including the formation and stability of the solid−electrolyte interface layer. Another issue that requires further consideration is the influence of the nanowire density on performance. Since the nanowire fabric has 90% void volume, the volumetric capacity of the nanowire fabric is relatively low. The specific capacity of 800 mA h g^{-1} corresponds to 186 mA h cm^{-3}, which is significantly lower than the volumetric capacity of 777−867 mA h cm^{-3} for graphite. However, it should be possible to increase the volumetric capacities of the nanowire fabric by densifying the films with pressure. An estimation of the maximum volumetric capacity of a densified Si nanowire fabric looks compelling, with a maximum of 1864 mA h cm^{-3}, which is more than a factor of 2 higher than that of graphite. The influence of volumetric expansion and contraction upon lithiation and delithiation on cycling stability, however, would still need to be understood.

ASSOCIATED CONTENT

Supporting Information. Movies (MPG) showing the fabrication and handling of Si nanowire fabric. This material is available free of charge via the Internet at http://pubs.acs.org.

AUTHOR INFORMATION

Corresponding Author
korgel@che.utexas.edu

ACKNOWLEDGMENT

We thank Kate Collier for HRTEM images of Si nanowires. Financial support of this research was provided in part by the Robert A. Welch Foundation (F-1464) and the Air Force Research Laboratory (FA-8650-07-2-5061). C.B.M. and K.J.S. acknowledge financial support from the Welch Foundation (F-1436 to C.B.M. and F-1529 to K.J.S.). V.C.H. acknowledges the Fannie and John Hertz Foundation and the National Science Foundation Graduate Research Fellowship Program for financial support. Raman spectroscopic characterization was supported as part of the program "Understanding Charge Separation and Transfer at Interfaces in Energy Materials (EFRC: CST)", an Energy Frontier Research Center funded by the U.S. Department of Energy, Office of Science, Office of Basic Energy Sciences, under Award DE-SC0001091.

REFERENCES

(1) Goodenough, J. B.; Kim, Y. *Chem. Mater.* **2010**, *22*, 587.
(2) Armand, M.; Tarascon, J. M. *Nature* **2008**, *451*, 652.
(3) Dahn, J. R.; Zheng, T.; Liu, Y.; Xue, J. S. *Science* **1995**, *270*, 90.
(4) Winter, M.; Besenhard, J. O.; Spahr, M. E.; Novák, P. *Adv. Mater.* **1998**, *10*, 725.
(5) Weydanz, W. J.; Wohlfahrt-Mehrens, M.; Huggins, R. A. *J. Power Sources* **1999**, *81*, 237.
(6) Obrovac, M. N.; Christensen, L. *Electrochem. Solid-State Lett.* **2004**, *7*, A93.
(7) Chan, C. K.; Peng, H.; Liu, G.; McIlwrath, K.; Zhang, X. F.; Huggins, R. A.; Cui, Y. *Nat. Nanotechnol.* **2008**, *3*, 31.
(8) Xu, Y. H.; Yin, G. P.; Zuo, P. J. *Electrochim. Acta* **2008**, *54*, 341.
(9) Boukamp, B. A.; Lesh, G. C.; Huggins, R. A. *J. Electrochem. Soc.* **1981**, *128*, 725.
(10) Chan, C. K.; Patel, R. N.; O'Connell, M. J.; Korgel, B. A.; Cui, Y. *ACS Nano* **2010**, *4*, 1443.
(11) Lee, J. K.; Smith, K. B.; Hayner, C. M.; Kung, H. H. *Chem. Commun.* **2010**, *46*, 2025.
(12) Graetz, J.; Ahn, C. C.; Yazami, R.; Fultz, B. *Electrochem. Solid-State Lett.* **2003**, *6*, A194.
(13) Kasavajjula, U.; Wang, C.; Appleby, A. J. *J. Power Sources* **2007**, *163*, 1003.
(14) Chan, C. K.; Ruffo, R.; Hong, S. S.; Huggins, R. A.; Cui, Y. *J. Power Sources* **2009**, *189*, 34.
(15) Hu, L.; Wu, H.; Hong, S. S.; Cui, L.; McDonough, J. R.; Bohy, S.; Cui, Y. *Chem. Commun.* **2010**, *47*, 367.
(16) Kang, K.; Lee, H.-S.; Han, D.-W.; Kim, G.-S.; Lee, D.; Lee, G.; Kang, Y.-M.; Jo, M.-H. *Appl. Phys. Lett.* **2010**, *96*, No. 053110.
(17) Laïk, B.; Eude, L.; Pereira-Ramos, J.-P.; Cojocaru, C. S.; Pribat, D.; Rouvière, E. *Electrochim. Acta* **2008**, *53*, 5528.
(18) Lee, J.-K.; Kung, M. C.; Trahey, L.; Missaghi, M. N.; Kung, H. H. *Chem. Mater.* **2009**, *21*, 6.
(19) Maranchi, J. P.; Hepp, A. F.; Kumta, P. N. *Electrochem. Solid-State Lett.* **2003**, *6*, A198.
(20) Peng, K.; Jie, J.; Zhang, W.; Lee, S.-T. *Appl. Phys. Lett.* **2008**, *93*, No. 033105.
(21) Huang, R.; Fan, X.; Shen, W.; Zhu, J. *Appl. Phys. Lett.* **2009**, *95*, No. 133119.
(22) Yao, Y.; McDowell, M. T.; Ryu, I.; Wu, H.; Liu, N.; Hu, L.; Nix, W. D.; Cui, Y. *Nano Lett.* **2011**, *11*, 2949.
(23) Heitsch, A. T.; Fanfair, D. D.; Tuan, H.-Y.; Korgel, B. A. *J. Am. Chem. Soc.* **2008**, *130*, 5436.
(24) Lee, D. C.; Hanrath, T.; Korgel, B. A. *Angew. Chem., Int. Ed.* **2005**, *44*, 3573.
(25) Holmes, J. D.; Johnston, K. P.; Doty, R. C.; Korgel, B. A. *Science* **2000**, *287*, 1471.
(26) Hanrath, T.; Korgel, B. A. *Adv. Mater.* **2003**, *15*, 437.
(27) Smith, D. A.; Holmberg, V. C.; Korgel, B. A. *ACS Nano* **2010**, *4*, 2356.
(28) Heitsch, A. T.; Akhavan, V. A.; Korgel, B. A. *Chem. Mater.* **2011**, *23*, 2697.
(29) Smith, D. A.; Holmberg, V. C.; Lee, D. C.; Korgel, B. A. *J. Phys. Chem. C* **2008**, *112*, 10725.

(30) de Heer, W. A.; Bacsa, W. S.; Châtelain, A.; Gerfin, T.; Humphrey-Baker, R.; Forro, L.; Ugarte, D. *Science* **1995**, *268*, 845.
(31) Endo, M.; Muramatsu, H.; Hayashi, T.; Kim, Y. A.; Terrones, M.; Dresselhaus, M. S. *Nature* **2005**, *433*, 476.
(32) Yuan, J.; Liu, X.; Akbulut, O.; Hu, J.; Suib, S. L.; Kong, J.; Stellacci, F. *Nat. Nanotechnol.* **2008**, *3*, 332.
(33) Holmberg, V. C.; Patel, R. N.; Korgel, B. A. *J. Mater. Res.* **2011**, *26*, 2305.
(34) Choi, J. W.; Hu, L.; Cui, L.; McDonough, J. R.; Cui, Y. *J. Power Sources* **2010**, *195*, 8311.
(35) Hu, L.; Wu, H.; La Mantia, F.; Yang, Y.; Cui, Y. *ACS Nano* **2010**, *4*, 5843.
(36) Ng, S. H.; Wang, J.; Guo, Z. P.; Chen, J.; Wang, G. X.; Liu, H. K. *Electrochim. Acta* **2005**, *51*, 23.
(37) Wang, J.-Z.; Zhong, C.; Chou, S.-L.; Liu, H.-K. *Electrochem. Commun.* **2010**, *12*, 1467.
(38) Tuan, H.-Y.; Korgel, B. A. *Chem. Mater.* **2008**, *20*, 1239.
(39) Saunders, A. E.; Sigman, M. B.; Korgel, B. A. *J. Phys. Chem. B* **2004**, *108*, 193.
(40) Choi, H. S.; Park, C. R. Towards High Performance Anodes with Fast Charge/Discharge Rate for LIB Based Electrical Vehicles. http://www.intechopen.com/articles/show/title/towards-high-performance-anodes-with-fast-charge-discharge-rate-for-lib-based-electrical-vehicles (accessed Sept 2, 2011).
(41) Obrovac, M. N.; Krause, L. J. *J. Electrochem. Soc.* **2007**, *154*, A103.
(42) Lopez, F. J.; Hemesath, E. R.; Lauhon, L. J. *Nano Lett.* **2009**, *9*, 2774.
(43) Davidson, F. M.; Lee, D. C.; Fanfair, D. D.; Korgel, B. A. *J. Phys. Chem. C* **2007**, *111*, 2929.
(44) Wang, R.-p.; Zhou, G.-w.; Liu, Y.-l.; Pan, S.-h.; Zhang, H.-z.; Yu, D.-p.; Zhang, Z. *Phys. Rev. B* **2000**, *61*, 16827.
(45) Hessel, C. M.; Rasch, M. R.; Hueso, J. L.; Goodfellow, B. W.; Akhavan, V. A.; Puvanakrishnan, P.; Tunnel, J. W.; Korgel, B. A. *Small* **2010**, *6*, 2026.
(46) Tuinstra, F.; Koenig, J. L. *J. Chem. Phys.* **1970**, *53*, 1126.
(47) Lespade, P.; Al-Jishi, R.; Dresselhaus, M. S. *Carbon* **1982**, *20*, 427.
(48) Ferrari, A. C.; Robertson, J. *Phys. Rev. B* **2000**, *61*, 14095.
(49) Ferrari, A. C. *Solid State Commun.* **2007**, *143*, 47.
(50) Monika, W.; Wang, Y.; Zerda, T. W. *J. Phys.: Condens. Matter* **2005**, *17*, 2387.
(51) Timmons, A.; Todd, A. D. W.; Mead, S. D.; Carey, G. H.; Sanderson, R. J.; Mar, R. E.; Dahn, J. R. *J. Electrochem. Soc.* **2007**, *154*, A865.